Dynamic response of a dual-frequency chiral hybrid aligned nematic liquid-crystal cell

S. A. Jewell and J. R. Sambles
Thin Film Photonics Group, School of Physics, University of Exeter, Stocker Road, Exeter EX4 4QL, United Kingdom
(Received 23 September 2005; published 17 January 2006)

The dynamic response of a chiral dual-frequency hybrid aligned nematic liquid-crystal cell to a multiple frequency pulse has been characterized using a time-resolved fully leaky guided-mode optical characterization technique. On application of a low-frequency voltage the cell is found to switch to homeotropic alignment, effectively destroying the inherent twist in the cell. When this voltage is immediately followed by a high-frequency voltage the structure is driven into a homogeneously aligned twisted structure. Analysis of the response of the director to this change in effective dielectric anisotropy of the material reveals a form of backflow. This arises due to the combination of the coupling between the rotation and flow of the director, the constraining effect of the pitch on the twist in the cell, and the driving of the director into homogeneous alignment. The measured director profiles have been compared to model profiles generated using the Leslie-Eriksen-Parodi nematodynamics theory, and the viscosity coefficients for the material have been determined.

DOI: 10.1103/PhysRevE.73.011706 PACS number(s): 61.30.Gd, 42.70.Df

I. INTRODUCTION

Current nematic liquid-crystal displays are hindered by the relatively slow response of the pixels to the removal of a voltage. High switch-on speeds are achievable due to the director being driven into the on-state by the application of an electric field, but the switch-off time is dictated by the mechanical and viscous forces acting on the material. The use of a dual-frequency nematic liquid crystal may go some way to solving this problem [1,2]. Such materials have dielectric anisotropies which are highly dependent on the frequency of the applied field; $\Delta\varepsilon(=\varepsilon_{\parallel}-\varepsilon_{\perp})$ can be positive, negative, or zero, depending on the frequency chosen. In particular, liquid-crystal compounds are available where the dielectric permittivity is highly dispersive, resulting in the dielectric anisotropy actually changing sign at a particular frequency referred to as the cross-over frequency, f_{co}. These materials can therefore be driven into an alignment either parallel or perpendicular to the direction of the applied field by simply changing the frequency of the voltage applied.

Previous work examining the dynamic properties of hybrid aligned nematic (HAN) cells has demonstrated that they have the potential for fast switching between homeotropic and homogeneous alignments. This arises due in part to the aligning layers providing an equal bias towards the two types of alignment, and also because such a structure exhibits thresholdless switching [3–5]. However, the transmission of light through a HAN cell (and subsequent homogeneous alignment produced on the application of a high-frequency voltage) is dictated by the optical birefringence of the material and is of limited use in a display. The contrast between homeotropic and homogeneous alignment when the cell is placed between crossed polarizers can be improved by adding a chiral dopant to the dual-frequency liquid crystal to produce a pitch which is comparable to four times the thickness of the cell to induce a 90 deg twist through the cell. The azimuth is dictated by the homogeneous alignment on one surface and the twist is unrestricted at the homeotropic surface, allowing the material to form a relatively unconstrained twist state [6,7]. For a suitably low concentration of chiral dopant, the material is able to maintain its dual-frequency properties, and so the structure can be switched from the 0 V chiral HAN (CHAN) structure (which both twists and tilts through approximately 90 deg) into either a homeotropically aligned state at low frequencies ($f<f_{co}$) or into a twisted homogeneous state of pitch comparable to the natural pitch of the material at high frequencies (Fig. 1). By applying a low-frequency pulse to switch the cell to homeotropic (appearing black under crossed polarizers) and then immediately applying a high-frequency pulse (to drive the cell into the twisted homogeneous light state) the cell can be driven between two optically very distinct alignments.

Optical wave-guide characterization provides a powerful method for probing the director structure inside a liquid-crystal cell [8–10]. A recently developed variant, referred to as the time-resolved fully leaky guided-mode (FLGM) technique [4], allows optical data collection on a submillisecond time scale while maintaining the extreme sensitivity to subtle changes in the director profile. This method is therefore ideal for studying the evolution of the dynamics of a CHAN cell on the application of a multiple-frequency pulse, and allows the complex director reorientation process to be examined in detail. It has been used here to study the complex dynamic procedures involved in the switching of a CHAN cell from 0 V to homeotropic alignment and then to a twisted-homogeneous structure. The results are compared to theoretical profiles generated using a nematodynamics model which incorporates a simple dual-frequency Debye-type model to describe the dielectric dispersion of the material.

II. EXPERIMENT

A hybrid cell of 4.94 μm thickness was constructed using indium-tin-oxide- (ITO) coated low-index ($n=1.52$) glass. One substrate was spin coated with a homogeneously aligning polymer, baked, and then rubbed to produce homogeneous alignment while the other was treated with a homeotropically aligning polymer and baked. The cell was then

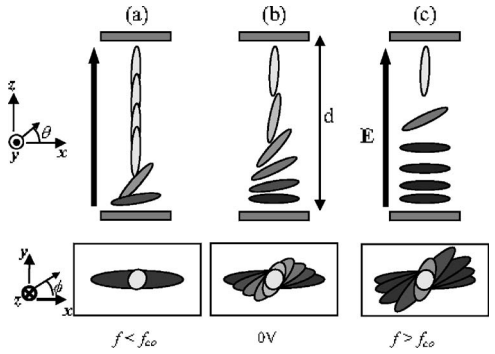

FIG. 1. Schematic diagram of the chiral HAN dual-frequency liquid crystal cell viewed in the *x*-*z* and *x*-*y* planes with (a) low-frequency high-voltage applied, (b) 0 V applied, and (c) high-frequency high-voltage applied.

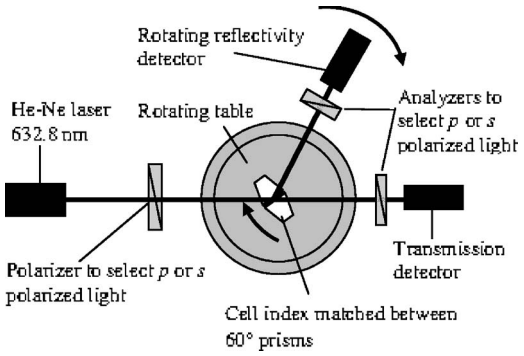

FIG. 2. Schematic diagram of the time-resolved fully leaky guided-mode experiment.

spaced using 5 μm glass beads dispersed in a UV curing glue along the edges.

A nonchiral nematic dual-frequency liquid crystal MLC-2048 (Merck KGa) was doped with 1.05% CB15 (Merck, KGa) by weight to produce a pitch of around 12.7 μm and the mixture was left in the isotropic phase for 24 h to allow complete mixing of the two components. The cell was then filled by capillary action in the isotropic phase and allowed to cool to room temperature before being sealed with an epoxy resin. A good monodomain was produced which showed no extinction in transmission when rotated in the *x*-*y* plane between crossed polarizers, demonstrating the presence of a cholesteric pitch.

The CHAN cell was refractive index-matched between two $n=1.52$, 60 deg prisms and mounted at the center of the time-resolved FLGM setup [4], as shown in Fig. 2. Optical intensity data were collected in reflection and transmission for polarization conserving and converting data on a 2 μs time scale and synchronized with the application of a multiple-frequency voltage pulse applied along the *z* axis of the cell through a LabVIEW interface. The pulse used was composed of a sinusoidal voltage of 7 V_{rms} at 2 kHz for 20 ms immediately followed by one of 7 V_{rms} at 64 kHz for 80 ms. This was repeated in 0.2 deg external incidence angle steps over an angle range (measured from the prism face and moving in the direction shown in Fig. 2) from 0 to 22 deg.

Once obtained, the data were sorted into sets of optical intensity versus angle-of-incidence for each time step and normalized. The optical data for selected time steps were fitted using a multi-layer optics model based on a 4×4 Berreman matrix [11] and a least-squares fitting procedure. In this model the optical permittivities, absorptivities, and the layer thicknesses of the ITO, homogeneous polyimide, homeotropic polyimide, and liquid crystal were used as fitting parameters, along with the twist, ϕ (measured anticlockwise from the *x* axis in the *x*-*y* plane), and tilt, θ (measured from the substrate), of the director orientation through the cell, described in both cases using second-order Bezier curves.

III. RESULTS AND ANALYSIS

To allow a meaningful comparison between measurements and modeling the twist and tilt profiles produced from the fitting procedure were converted into the n_x, n_y, and n_z components of the director (unit vector **n**), being defined as

$$n_x = \cos\theta\cos\phi,$$

$$n_y = \cos\theta\sin\phi,$$

$$n_x = \sin\theta. \tag{1}$$

This notation has been chosen, rather than the conventional method of considering the tilt and twist independently, due to complications encountered when the director becomes homeotropic. In this case, $\theta=90$ deg and hence there is no projection of the director onto the *x*-*y* plane, resulting in the twist being undefined. However, if the *n*-director notation is used, $n_z=1$ and $n_x=n_y=0$ resulting in all three components being well defined.

To enable a greater understanding of the response of the director at different points through the cell, Fig. 3 shows the measured n_x, n_y, and n_z components at points 1, 2, 3, and 4 μm through the cell plotted as a function of time. The results clearly show that the reorientation of the tilt (i.e., n_z) dominates the initial response of the liquid crystal to a change in the frequency of the applied voltage, with the twist reorientation (manifest in n_x and n_y) being a secondary response on a much longer time scale. This is to be expected, as the electric field is applied solely along the *z* axis, and hence there is no dielectric torque component acting in the plane of the twist. The reorientation of the twist is dictated by the visco-elastic forces in the system, as discussed in detail later, and this response is analogous to the slow switch-off response of the tilt in a nontwisted HAN cell when a voltage is removed [12].

The variation of the director profile during the dual-frequency switching of the cell can be modeled using the Leslie-Eriksen-Parodi theory [13,14] to model the switch-on of the CHAN cell from 0 V to the twisted-homeotropic state initially using the low-frequency value for $\Delta\varepsilon$ in the model. At the time when the frequency is switched (20 ms), the value of $\Delta\varepsilon$ used in the simulation is switched to the high-frequency value (assuming an instantaneous response to the change in frequency) and the switch-off director profile can be calculated.

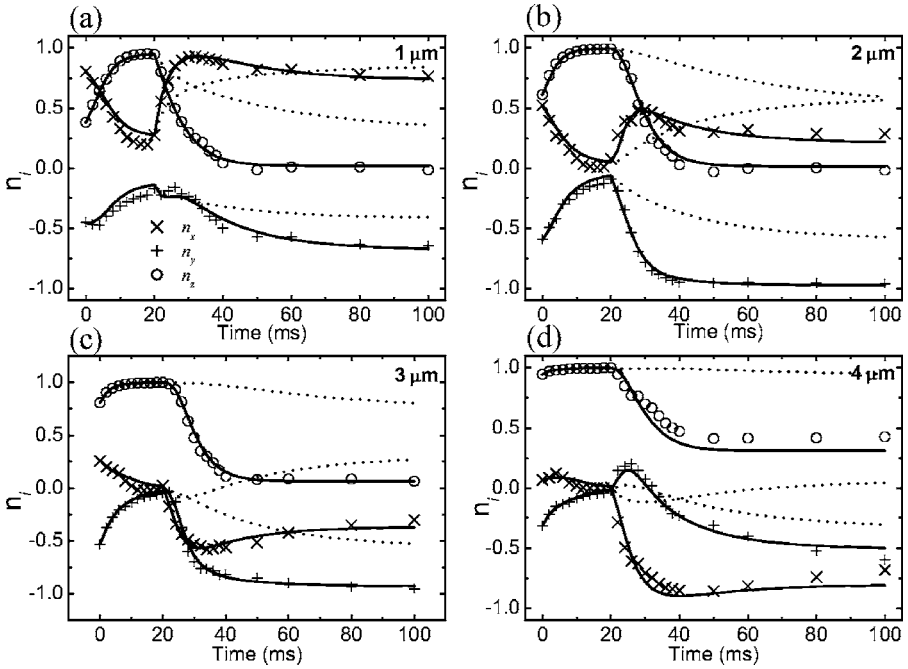

FIG. 3. Comparison of measured (symbols) and modeled (lines) of the time evolution of n_x, n_y, and n_z at points (a) 1 μm, (b) 2 μm, (c) 3 μm, and (d) 4 μm through the cell. A low-frequency field (2 kHz) is applied between $t=0$ and $t=20$ ms and a high-frequency field (64 kHz) is applied between $t=20$ ms and $t=100$ ms. The values of the physical constants used are stated in the text. The dotted lines show the modeled natural relaxation of the cell when the voltage is removed at $t=20$ ms.

The approach used is based on work by Van Doorn [15] and uses the nematodynamic theory described in detail in the Appendix. Generally, for a nontwisted 1D structure these equations of motion can be greatly simplified [16] as there is no change in the twist orientation, so one can arbitrarily assume that the director remains in the x-z plane throughout. In this case only n_x and n_z vary and the dynamic process and the equations of motion are only dependent on the tilt allowing the equations to be expressed in terms of θ and its spatial and temporal derivatives. However, for the CHAN cell, both twist and tilt must be considered along with a coupling between the two so simplification into one plane is not possible. In addition, due to the twist becoming undefined as the tilt becomes homeotropic, to ensure stability when calculating the director dynamics it is important to use the three n-director variables (and their derivatives) rather than converting them into the two individual twist and tilt components. The iterative procedure implemented in the calculations used to solve these equations to determine the director dynamics is presented in detail in the Appendix. The general procedure is that the initial director configuration at time $t=t_o=0$, determined through either optical measurements of the cell under test or by using a free-energy minimization model, is used as the starting point. Values for $\dot{n}_i$ (where $i=x$, y, or z) are guessed and then refined through an iterative process and then the Cranks-Nicholson method [17] is used to determine the new director profile at time $t'=t_o+\Delta t$. This director profile is then set as the new starting profile and the whole process is repeated until the time duration of the first frequency section of the multiple frequency pulse is reached. This profile is then set as the new starting profile, and the value of the dielectric anisotropy associated with the frequency of the second section of the voltage pulse is used in the dynamics equations and the process continues as before.

In practice, a Debye model was used to describe the dielectric dispersion of the material [3,18], with the frequency, rather than the actual dielectric anisotropy, being used as an input parameter. The advantage of this is that the phase and amplitude of the voltage could be used to describe the time-varying field within the cell (assuming the absence of free charges). Therefore, in the cases where a voltage with a period of the order of, or less than, the response time of the liquid crystal director is used, the director can be observed to follow the applied field.

The results of modeling the director response for the dual-frequency CHAN cell are shown as the solid lines in Fig. 3. The coefficients used in the modeling are $k_{11}=16.7(\pm1)$ pN, $k_{22}=10.0(\pm2)$ pN, $k_{33}=20.9(\pm1)$ pN, and pitch$=13.0(\pm1)$ μm. The dielectric anisotropies used are $\Delta\varepsilon(2\text{ kHz})=2.6(\pm0.1)$ and $\Delta\varepsilon(64\text{ Hz})=-2.3(\pm0.1)$ and the Miesowicz viscosity coefficients (defined using the Helfrich notation) used are $\gamma_1=0.30(\pm0.02)$ Pas, $\eta_1=0.33(\pm0.02)$ Pas, $\eta_2=0.055(\pm0.02)$ Pas, $\eta_3=0.085(\pm0.02)$ Pas, and $\eta_{12}=-0.01(\pm0.01)$ Pas.

The fits presented were obtained by manually adjusting these parameters in the nematodynamics model until a reasonable fit was obtained to the director evolution at the four selected points in the cell. Exploring the data in this way enabled a clearer method of ascertaining which physical parameters affected which parts of the cell. For example, the ratio η_2/η_3 influenced the form of the peak that occurs in the n_y component towards the homeotropic surface (at ~4 μm) immediately after the frequency is switched, whereas towards the center of the cell (around 2 and 3 μm) the rate of change of n_x after the application of the 64 kHz pulse is sensitive to the value of k_{22}. In general, the final value of n_z at the end of each pulse section is dictated by the dielectric anisotropy of the material at 2 and 64 kHz and the form of the reorientation is dominated by γ_1. Varying the other viscosity coefficients by ±50% (while obeying the inequalities governing the relative values that these coefficients can take [19]) had a negligible effect on the n_z profiles, hence the relatively large uncertainties in the figures quoted. The slight discrepancies between the measured and modeled variations

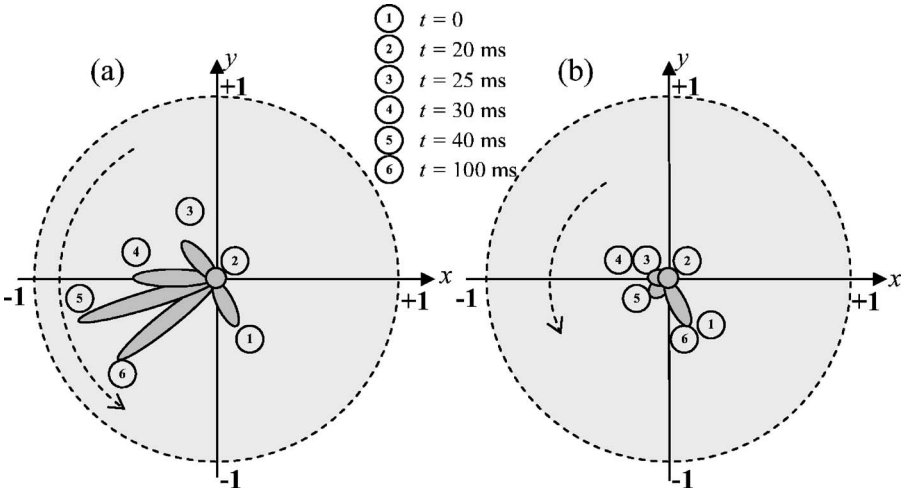

FIG. 4. Schematic representation of the motion of the director, projected onto the *x*-*y* plane for switching a dual-frequency CHAN cell into homeotropic alignment (0 to 20 ms) and then (a) driving it into the twisted nematic state using a high-frequency pulse or (b) allowing it to relax into the 0 V state on removal of the voltage.

of n_i with time can be partially attributed to the rigid anchoring approximation used in the dynamics model. In addition, the measured director components were obtained by using a mathematical curve, rather than a physical model, to approximate the form of the director profile through the cell. The discrepancies are particularly noticeable in the second half of the cell (towards the homeotropic end) which is likely to be due to the FLGM technique having a higher sensitivity to the region closest to the incident substrate.

A backflow effect produced when the frequency of the applied field is switched can be seen in Fig. 3(d) when the signs of n_x and n_y are considered. This is illustrated as a projection onto the *x*-*y* plane in Fig. 4(a). The value of n_y is initially negative at 0 V and n_x is positive. When the cell switches to homeotropic alignment the magnitude of both components decreases to near zero as the projection of the director on the *x*-*y* plane is reduced, and to a first-order approximation ϕ is undefined. On application of the high-frequency section of the pulse, however, n_y immediately becomes positive for around 10 ms before switching back to negative for the remainder of the pulse duration, while n_x switches to negative immediately and continues to increase in magnitude throughout the high-frequency pulse duration. At the start of the voltage application ($t_o=0$) and during the entire homeotropic aligning process the director remains solely in the lower right quadrant, as shown. At time $t=20$ ms the director is almost totally homeotropic and hence centered at the origin of the graph. On application of the high-frequency section, the director immediately moves into the top left quadrant, which must be achieved by the director "falling backwards." This results in the twist, measured clockwise from the *x* axis, instantly increasing by around 180 deg at this point in the cell. The director is then driven down towards the substrate by the action of the applied field while simultaneously the twist reduces in magnitude as the influence of the pitch and k_{22} draws the cell back into its naturally twisted equilibrium state. This can clearly be seen in Fig. 5 which shows the complete evolution of the modeled tilt and twist profiles during the switching processes. Figure 5(d) shows an initial jump in the twist of 180 deg on application of the high frequency, while Fig. 5(c) demonstrates an oscillation in the tilt (measured from the *x*-*y* plane) corresponding to the over-rotation of the director. This initial response of the director close to the homeotropic surface is analogous to the backflow mechanism occurring in the relaxation of a nontwisted HAN cell filled with a positive dielectric anisotropy material [12]. On removal of the field inducing the homeotropic alignment the elastic torque in the bulk of the cell induces a rapid rotation towards homogeneous alignment which induces a shear flow in the *x* direction in the less highly strained homeotropic region, resulting in a counter-rotation before relaxing back into the 0 V state. However, in the case of the chiral structure shear flow is induced in both the *x* and *y* directions due to the twist and once the director has started to over-rotate the action of the high-frequency field causes the director to continue in that direction.

The influence of the effect of driving the director into homogeneous alignment on the backflow can be seen when it is compared to modeling of the undriven natural relaxation of the cell when the cell is switched to homeotropic and the voltage is then removed. The dotted lines in Fig. 3 show this effect, using the same parameters as in the previous modeling, and a schematic diagram of the corresponding director projection in the *x*-*y* plane at 4 μm through the cell is shown in Fig. 4(b). In the natural relaxation case a very small amount of backflow occurs on removal of the voltage causing the director to over-rotate, adding an extra 180 deg to the twist, but due to the director remaining close to the homeotropic state throughout (due to its proximity to the homeotropic substrate) this twist is relatively insignificant.

The final values of n_x, n_y, and n_z reached in the undriven relaxation at all points through the cell in Fig. 3 shows good agreement with the original 0 V starting points which confirms the suitability of the elastic coefficients used (neglecting flexo-electric contributions). Furthermore, the values show reasonable agreement with the measured values of $k_{11}=15(\pm1)$ pN and $k_{33}=20(\pm1)$ pN obtained from Frederickszs transition measurements on pure MLC-2048-000 at 25 °C, with the discrepancies between the two likely to be due to the influence of the chiral dopant material on the elastic constants and the slight temperature difference. The measured value of k_{22} appears high when compared to values for other nematic liquid crystals, but the ratio of the bend and twist coefficients measured here ($k_{33}/k_{22}=2.09$) is reasonable for a nematic material.

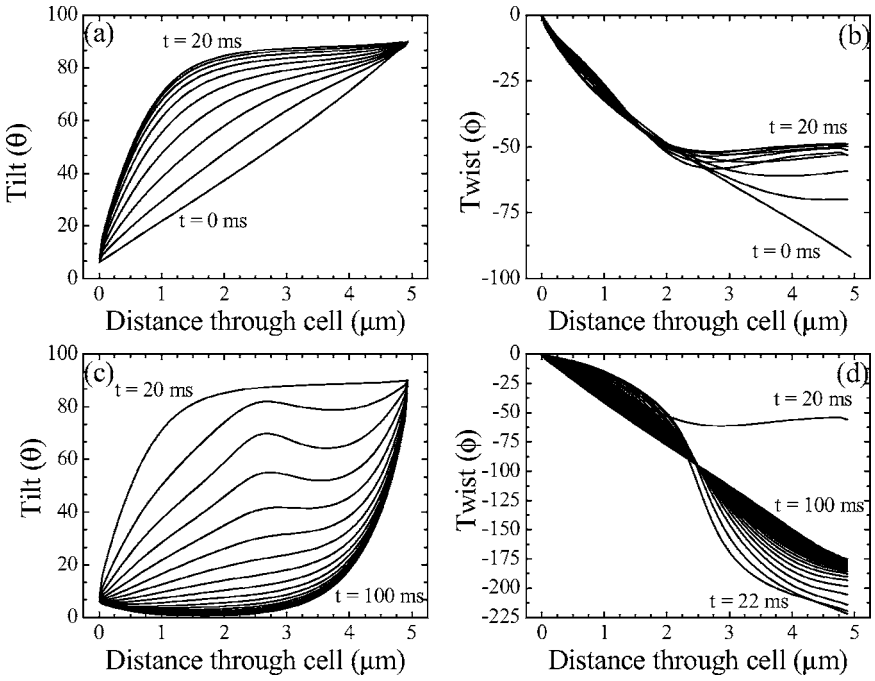

FIG. 5. Modeled evolution of the twist and tilt profiles (deg) of the director with time during the low-frequency switching to the homeotropic state [(a) and (b)] and the high-frequency switching to the twisted homogeneous alignment [(c) and (d)].

IV. CONCLUSION

The combination of a chirally doped dual-frequency nematic liquid crystal with a hybrid alignment structure has been shown to allow the director to be driven between homeotropic and twisted homogeneous alignment. The use of a multiple frequency pulse to drive the director between the two states has revealed a form of backflow occurring when the frequency is switched from below the crossover frequency of the material to above it. This arises initially due to the overrotation of the tilt close to the homeotropic surface due to a coupling between rotation and flow, but it is then driven further by the combined effect of the negative dielectric anisotropy of the material at high frequencies and the pitch induced by the chiral dopant. The measured response of the cell shows good agreement with theoretical profiles generated using the Leslie-Eriksen-Parodi theory with flow in two dimensions. In this study the gain in response time achieved by the fast switching to the homogeneous state is compromised by the slow undriven response of the twist, but with the use of a dual-frequency with optimized elastic and viscosity coefficients, such a structure may be suitable for use in a liquid crystal display.

ACKNOWLEDGMENTS

The authors would like to thank Dr. C. V. Brown of Nottingham Trent University, UK for the dielectric anisotropy and elastic constant measurements. This project forms part of a COMIT Faraday partnership funded by the Engineering and Physical Sciences Research Council and the DTI.

APPENDIX

From the nematodynamics theory of Eriksen and Leslie [13,14] and using the approach of Vertogen and de Jeu [20], the flow in an anisotropic fluid is governed by two equations. First, there is the Navier-Stokes equation:

$$\rho \dot{v}_i = F_i + \sigma_{ji,j},$$

where $i=x,y$, or z, F_i is the external body force acting on the fluid (e.g., gravitation), and ρ is the density of the fluid. $\sigma_{ji,j}$ is the differential of the jith element of the stress tensor, σ_{ji}, with respect to j, and $\dot{v}_i$ is the rate of change of the flow velocity $\mathbf{v}$ in the i direction with respect to time. The stress tensor is defined as

$$\sigma_{ji} = -p\partial_{ij} - \frac{\partial F}{\partial n_{k,j}} n_{k,i} + \alpha_1 n_k n_p A_{kp} n_i n_j + \alpha_2 n_j N_i + \alpha_3 n_i N_j + \alpha_4 A_{ij} + \alpha_5 n_j n_k A_{ki} + \alpha_6 n_i n_k A_{kj},$$

where the six Leslie coefficients are denoted by α_n. A_{ij} is the symmetric part of the flow gradient tensor, $A_{ij}=\frac{1}{2}(v_{i,j}+v_{j,i})$, and N_i contains the antisymmetric part, $N_i=\dot{n}_i+\frac{1}{2}n_j(v_{i,j}-v_{j,i})$. In all cases, $n_i \equiv n_i(z,t)$, $\dot{n}_i \equiv \dot{n}_i(z,t)$, and $v_i \equiv v_i(z,t)$.

As F_i is negligible this term can be ignored, and due to the inertial terms acting over a time scale several orders of magnitude smaller than that of the overall response of the cell these terms can be neglected (i.e., $\rho\dot{v}_i=0$). For a 1D system with variation along the z axis, only the cases where $j=z$ are nonzero, and neglecting the situation where $i=z$ to avoid complexities produced due to the inclusion of hydrostatic pressure, two equations result, $\sigma_{zx,z}=0$ and $\sigma_{zy,z}=0$, which are given by

$$0 = \frac{\partial}{\partial z}\left(\alpha_2 \dot{n}_x n_z + \alpha_3 \dot{n}_z n_x + \frac{1}{2}\alpha_3 n_x n_y v_y' + \frac{1}{2}(2\alpha_1 n_x^2 n_z^2 - \alpha_2 n_z^2 + \alpha_3 n_x^2 + \alpha_4 + \alpha_5 n_z^2 + \alpha_6 n_x^2) v_x' \right), \tag{A1}$$

$$0 = \frac{\partial}{\partial z}\left(\alpha_2 \dot{n}_y n_z + \alpha_3 \dot{n}_z n_y + \frac{1}{2}\alpha_3 n_y n_x v_x' + \frac{1}{2}(2\alpha_1 n_y^2 n_z^2 - \alpha_2 n_z^2 + \alpha_3 n_y^2 + \alpha_4 + \alpha_5 n_z^2 + \alpha_6 n_y^2) v_y' \right). \tag{A2}$$

The second expression comes from the Euler-Lagrange equation of motion:

$$\rho_1 \ddot{n}_i = G_i + g_i + \pi_{ji,j}.$$

ρ_1 is the moment of inertia per unit volume associated with the director (assumed to be zero in all cases), G_i is the external body torque, in this case exerted by the applied field, and hence $G_x = G_y = 0$ and $G_z = \varepsilon_o \Delta\varepsilon E^2 n_z$ as the field is only along the z axis. The director surface torque is defined as $\pi_{ji} = \partial F / \partial n_{i,j}$ and only the components where $j = z$ are nonzero. g_i is the internal body torque per unit volume and is defined as

$$g_i = \gamma n_i - \frac{\partial F}{\partial n_i} - \gamma_1 N_i - (\alpha_3 + \alpha_2) n_j A_{ji},$$

where γ is a Lagrangian multiplier to ensure the constraint that $n_x^2 + n_y^2 + n_z^2 = 1$. The free-energy density of the system, F, comes from the standard continuum theory where

$$F = \frac{1}{2}k_{11}(\nabla \cdot \mathbf{n})^2 + \frac{2\pi}{p}k_{22}(\mathbf{n} \cdot \nabla \times \mathbf{n}) + \frac{1}{2}k_{22}(\mathbf{n} \cdot \nabla \times \mathbf{n})^2 + \frac{1}{2}k_{33}(\mathbf{n} \times \nabla \times \mathbf{n})^2,$$

with the splay, twist and bend elastic constants given by k_{11}, k_{22}, and k_{33}, respectively, and p being the natural cholesteric pitch of the material. The three equations from the Euler-Lagrange equation of motion written out explicitly are therefore

$$0 = \gamma n_x - \frac{\partial F}{\partial n_x} + \frac{\partial}{\partial z}\frac{\partial F}{\partial n_{x,z}} - \gamma_1 \dot{n}_x - \alpha_2 n_z v_x' = \gamma n_x - \gamma_1 \dot{n}_x + G(n_i, v_x') \tag{A3}$$

$$0 = \gamma n_y - \frac{\partial F}{\partial n_y} + \frac{\partial}{\partial z}\frac{\partial F}{\partial n_{y,z}} - \gamma_1 \dot{n}_y - \alpha_2 n_z v_y' = \gamma n_y - \gamma_1 \dot{n}_y + H(n_i, v_y'), \tag{A4}$$

$$0 = \gamma n_z - \frac{\partial F}{\partial n_z} + \frac{\partial}{\partial z}\frac{\partial F}{\partial n_{z,z}} + \varepsilon_o \Delta\varepsilon E^2 n_z - \gamma_1 \dot{n}_z - \alpha_3 n_x v_x' - \alpha_3 n_y v_y' = \gamma n_z - \gamma_1 \dot{n}_z + I(n_i, v_y', v_x'). \tag{A5}$$

Combining Eqs. (A3) and (A4) to eliminate γ gives

$$0 = \gamma_1(n_x \dot{n}_y - n_y \dot{n}_x) + n_x H(n_i, v_y') - n_y G(n_i, v_x'), \tag{A6}$$

and, similarly,

$$0 = \gamma_1(n_x \dot{n}_z - n_z \dot{n}_x) + n_x I(n_i, v_y', v_x') - n_z G(n_i, v_x'), \tag{A7}$$

$$0 = \gamma_1(n_y \dot{n}_z - n_z \dot{n}_y) + n_z H(n_i, v_y') - n_y I(n_i, v_y', v_x'). \tag{A8}$$

Differentiating the constraint $n_x^2 + n_y^2 + n_z^2 = 1$ with respect to time and rearranging gives

$$\dot{n}_y = -\frac{1}{n_y}(n_x \dot{n}_x + n_z \dot{n}_z).$$

Putting this into Eq. (A6), multiplying through by n_y / n_z, and then adding to Eq. (A7) gives

$$0 = \gamma_1(n_x^2 + n_y^2 + n_z^2)\dot{n}_x - n_x n_y H(n_i, v_y') - n_x n_z I(n_i, v_y', v_x') + (n_y^2 + n_z^2) G(n_i, v_x'),$$

and so the rate of change of n_z at this instance in time is

$$\dot{n}_x = \frac{1}{\gamma_1}[n_x n_y H(n_i, v_y') + n_x n_z I(n_i, v_y', v_x') - (n_y^2 + n_z^2) G(n_i, v_x')]. \tag{A9}$$

Similarly for n_y and n_z the time variation is

$$\dot{n}_y = \frac{1}{\gamma_1}[n_x n_y G(n_i, v_x') - n_y n_z I(n_i, v_y', v_x') + (n_z^2 - n_x^2) H(n_i, v_y')], \tag{A10}$$

$$\dot{n}_z = \frac{1}{\gamma_1}[n_x n_z G(n_i, v_x') - n_y n_z H(n_i, v_y') + (n_y^2 - n_x^2) I(n_i, v_y', v_x')]. \tag{A11}$$

Integrating Eqs. (A1) and (A2) with respect to z gives two integration constants, C_1 and C_2, which are fixed by the nonslip boundary conditions $v_x(0) = v_y(0) = v_x(d) = v_y(d) = 0$. Hence

$$C_1 = \alpha_2 \dot{n}_x n_z + \alpha_3 \dot{n}_z n_x + \left(\frac{1}{2}\alpha_3 n_x n_y\right) v_y' + \frac{1}{2}(2\alpha_1 n_x^2 n_z^2 - \alpha_2 n_z^2 + \alpha_3 n_x^2 + \alpha_4 + \alpha_5 n_z^2 + \alpha_6 n_x^2) v_x',$$

$$C_2 = \alpha_2 \dot{n}_y n_z + \alpha_3 \dot{n}_z n_y + \left(\frac{1}{2}\alpha_3 n_y n_x\right) v_x' + \frac{1}{2}(2\alpha_1 n_y^2 n_z^2 - \alpha_2 n_z^2 + \alpha_3 n_y^2 + \alpha_4 + \alpha_5 n_z^2 + \alpha_6 n_y^2) v_y'.$$

Grouping terms for succinctness produces two expressions dependent on the director orientation and the rate of change of the orientation with time:

$$C_1 = A(n_x,n_z,\dot{n}_x,\dot{n}_z) + B(n_x,n_y)v_y' + C(n_x,n_z)v_x', \quad \text{(A12)}$$

$$C_2 = D(n_y,n_z,\dot{n}_y,\dot{n}_z) + B(n_x,n_y)v_x' + E(n_y,n_z)v_y'. \quad \text{(A13)}$$

Combining these expressions produces expressions for the velocity gradient for the x and y components of the flow:

$$v_x' = \frac{E(n_y,n_z)C_1 - B(n_x,n_y)C_2 - A(n_x,n_z,\dot{n}_x,\dot{n}_z)E(n_y,n_z) + B(n_x,n_y)D(n_y,n_z,\dot{n}_y,\dot{n}_z)}{C(n_x,n_z)E(n_y,n_z) - [B(n_x,n_y)]^2}, \quad \text{(A14)}$$

$$v_y' = \frac{C(n_x,n_z)C_2 - B(n_x,n_y)C_1 + A(n_x,n_z,\dot{n}_x,\dot{n}_z)B(n_x,n_y) - C(n_x,n_z)D(n_y,n_z,\dot{n}_y,\dot{n}_z)}{C(n_x,n_z)E(n_y,n_z) - [B(n_x,n_y)]^2}. \quad \text{(A15)}$$

The values of n_x, n_y, and n_z are known at time $t_o=0$ (i.e., the static profile before any field is applied) and an initial "guess" of the rate of change of the director with respect to time [e.g., $\dot{n}_x(z,t_o)=\dot{n}_y(z,t_o)=\dot{n}_z(z,t_o)=0$] can be made. From the nonslip boundary conditions $\int_0^d v_x'dz=\int_0^d v_y'dz=0$ Eqs. (A14) and (A15) can be integrated numerically with respect to z at time $t_o=0$ to obtain two simultaneous equations allowing C_1 and C_2 to be determined. These values are then used in Eqs. (A14) and (A15) to calculate $v_x'(z,t_o)$ and $v_y'(z,t_o)$ for each required point through the cell. Finally, using Eqs. (A9)–(A11), newly refined values for $\dot{n}_x$, $\dot{n}_y$, and $\dot{n}_z$ can be determined. These values are then used as the new "guessed" value for the rate of change of the director with respect to time in Eqs. (A14) and (A15) and the process is repeated around 100 times until final values of $\dot{n}_x(z,t_o)$, $\dot{n}_y(z,t_o)$, and $\dot{n}_z(z,t_o)$ are converged on.

The next stage involves using the Cranks-Nicolson method [17] to determine the new director profile $\mathbf{n}(z,t')$ at time $t'=t_o+\Delta t$. The first step involves calculating an initial approximation of the new director profile using $n_i(z,t')=n_i(z,t_o)+\dot{n}_i(z,t_o)\Delta t$ for each point through the cell. To maintain the condition that $|\mathbf{n}(z,t')|=1$, it is essential to evaluate $r^2=[n_x(z,t')]^2+[n_y(z,t')]^2+[n_z(z,t')]^2$ and then renormalize the newly calculated director components by using $\tilde{n}_i(z,t')=n_i(z,t')/r$. The Cranks-Nicolson routine can be summarized as follows. The rate of change of the director at time t' is calculated using the iterative process as before, starting with $\dot{n}_i(z,t_o)$ as the initial guess in Eqs. (A14) and (A15). (In these calculations, when using an ac field, the new value of the amplitude of the voltage at time t' is calculated, assuming the voltage is of the form $V(t)=V_0\sin(2\pi ft)$). On convergence of $\dot{n}_i(z,t')$, the new director profile at time t' is calculated using $n_i(z,t')=n_i(z,t_o)+(\Delta t/2)[\dot{n}_i(z,t_o)+\dot{n}_i(z,t')]$ and then using the renormalizing step as before. This is the end of the calculation for the first time step, and the entire process is started again using these values as the "known" director profile and calculating the new director profile at time Δt later.

In practice, it was found that using time steps of 2 μs was adequate for producing a sufficiently smooth time evolution of the profile. Also, the change to the director components by renormalizing after each time step was extremely small (usually a factor of around 10^{-10}), although significant enough to cause instabilities after a few thousand iterations if the director was left unnormalized.

[1] M. Schadt, Annu. Rev. Mater. Sci. **27**, 305 (1997).
[2] E. P. Raynes and I. Shanks, Electron. Lett. **10**, 114 (1974).
[3] S. A. Jewell and J. R. Sambles, Opt. Express **13** (7), 2627 (2005).
[4] S. A. Jewell, T. S. Taphouse, and J. R. Sambles, Appl. Phys. Lett. **87**, 021106 (2005).
[5] Y. Q. Lu, X. Liang, Y. H. Wu, F. Du, and S. T. Wu, Appl. Phys. Lett. **85**, 16 (2004).
[6] M. R. Lewis and M. C. K. Wiltshire, Appl. Phys. Lett. **51**, 1197 (1987).
[7] Y. J. Kim and S. D. Lee, Appl. Phys. Lett. **72**, 1978 (1998).
[8] F. Z. Yang and J. R. Sambles, J. Opt. Soc. Am. B **16**, 3 (1999).
[9] S. A. Jewell and J. R. Sambles, J. Appl. Phys. **92**, 1 (2002).
[10] S. A. Jewell, J. R. Sambles, J. W. Goodby, A. W. Hall, and S. J. Cowling, J. Appl. Phys. **95**, 5 (2004).
[11] D. Y. K. Ko and J. R. Sambles, J. Opt. Soc. Am. A **5**, 1863 (1988).
[12] S. A. Jewell and J. R. Sambles, Appl. Phys. Lett. **82**, 19 (2003).
[13] J. L. Eriksen, Arch. Ration. Mech. Anal. **9**, 371 (1962).
[14] F. M. Leslie, Q. J. Mech. Appl. Math. **19**, 357 (1966).
[15] C. Z. Van Doorn, J. Appl. Phys. **46**, 9 (1975).
[16] H. G. Walton and M. J. Towler, Liq. Cryst. **27**, 10 (2000).
[17] W. H. Press *et al.*, *Numerical Recipes in Fortran: The Art of Scientific Computing*, 2nd ed. (Cambridge University Press, Cambridge, 1992).
[18] Y. Yin, S. Shiyanovskii, A. B. Golovin, and O. D. Lavrentovich, Phys. Rev. Lett. **95**, 087801 (2005).
[19] I. W. Stewart, *The Static and Dynamic Continuum Theory for Liquid Crystals* (Taylor and Francis, London, 2004).
[20] G. Vertogen and W. H. de Jeu, *Thermotropic Liquid Crystals, Fundamentals* (Springer-Verlag, Berlin, 1988).